Journal of Power Sources 242 (2013) 264–272

Contents lists available at SciVerse ScienceDirect

Journal of Power Sources

journal homepage: www.elsevier.com/locate/jpowsour

Comprehensive study of an air bleeding technique on the performance of a proton-exchange membrane fuel cell subjected to CO poisoning

Lung-Yu Sung [a,b], Bing-Joe Hwang [a,*], Kan-Lin Hsueh [b,d], Wei-Nien Su [c], Chang-Chung Yang [b]

[a] Department of Chemical Engineering, National Taiwan University of Science and Technology, Taipei 106, Taiwan
[b] Green Energy and Environment Research Laboratories, Industrial Technology Research Institute, Hsinchu 310, Taiwan
[c] Graduate Institute of Applied Science and Technology, National Taiwan University of Science and Technology, Taipei 106, Taiwan
[d] Department of Energy Engineering, National United University, Miaoli 360, Taiwan

HIGHLIGHTS

- This study covers various temperatures, air bleeding, cell voltages, and CO levels.
- A 5% air bleeding recovers 90% cell performance, even at 200 ppm CO.
- Proposed model well fits to CO poisoning data at various operating conditions.
- Cell degradation is less than 2% in a 300-hr, 5% air bleed durability test.

ARTICLE INFO

Article history:
Received 6 March 2013
Received in revised form
24 April 2013
Accepted 10 May 2013
Available online 18 May 2013

Keywords:
Proton-exchange membrane fuel cell
Carbon monoxide poisoning
Air bleeding
Combined heat and power

ABSTRACT

CO poisoning is a major issue for proton-exchange membrane fuel cells (PEMFCs) when reformate gas is used as a fuel, especially at low temperatures (<80 °C). The performance of a PEMFC is investigated when subject to CO poisoning under different operation conditions and a simplified model is hereby proposed. It is found that even when the a CO-tolerant material like platinum–ruthenium (Pt–Ru) is used as the anode catalyst, the cell loses approximately 40% of its current density within 40 min with hydrogen fuel containing 25 ppm CO. By applying 5% air bleeding, the cell output current can be restored to 90% within 10 min, even at high CO concentrations (200 ppm). However, excessive air bleeding (>10% air) also reduces the cell output power. Based on impedance measurements, CO poisoning can strongly increase the charge transfer resistance without affecting the cell internal resistance. The stability test for 300 h using 200 ppm CO and 5% air bleeding shows that the cell power output can remain stable with the overall degradation less than 2%. From the viewpoints of system design and operation, air bleeding offers a stable power output and allows for a simpler, smaller, and cheaper reformer.

1. Introduction

Proton-exchange membrane fuel cells (PEMFCs) have many advantages over other fuel cells, such as high power density, quick start-up, low operating temperatures (<80 °C), and low emission of greenhouse gases. PEMFCs have been successfully demonstrated as a viable electrical power source for stationary, transportation, and portable applications. Hydrogen or hydrocarbon-based fuels can be used for the anode. High power densities (>1.0 W cm^{-2}) have been achieved using pure hydrogen as the fuel (from pressurised hydrogen, liquid hydrogen, or metal hydrides). However, applications using pure hydrogen in PEMFCs are limited due to technical barriers such as hydrogen storage, delivery, infrastructure, and safety regulations.

PEMFCs can also use hydrocarbons (i.e., natural gas, methanol, ethanol, and diesel) as the anode fuel. Hydrogen-rich reformate gas (containing about 45–75 vol.% hydrogen) can be obtained by reforming these hydrocarbon fuels [1]. Because these chemicals are commonly used in daily life, the infrastructure for their distribution, storage, safety, and regulation are well-established. PEMFCs using hydrocarbon fuels have been widely used for residential combined heat and power (CHP) applications [2–4], but the power systems require reformer systems. PEMFC-based power systems provide enough electrical power (1–5 kW) and heat for a typical family home. However, reformate gas produced by reforming hydrocarbons contains a small amount of carbon monoxide (CO). Although the water-

* Corresponding author. Tel.: +886 2 27376624; fax: +886 2 27376644.
E-mail address: bjh@mail.ntust.edu.tw (B.-J. Hwang).

0378-7753/$ – see front matter © 2013 Published by Elsevier B.V.
http://dx.doi.org/10.1016/j.jpowsour.2013.05.042

gas shift reaction (WGSR) and CO preferential oxidation (PROX) technique can reduce the CO content to a few ppm (10–50 ppm) [5,6], the cell performance is significantly reduced even when the fuel gases contain only 5 ppm CO [7–9]. The main catalyst used in PEMFCs is platinum (Pt). Pt is a superb catalyst for the hydrogen oxidation reaction (HOR, $H_2 \rightarrow 2H^+ + 2e^-$) and is chemically stable in the PEMFC operating environment. However, the CO molecules are prone to being adsorbed on the Pt catalyst surface and cause severe CO poisoning at low temperatures [10,11], leading to a loss of catalytic activity and a significant reduction in fuel cell performance. Therefore, although using PEMFCs with hydrocarbon fuels have many advantages, the CO poisoning effect remains a major challenge that needs to be resolved before their commercialisation in CHP applications.

The CO poisoning phenomenon has been extensively studied, and several approaches have been proposed to mitigate the CO poisoning of PEMFC anodes [5–33]. These approaches include pretreatment of the reformate gas [5,6,10–13], pulsed oxidation for the regeneration of CO-poisoned cells [14–16], air bleeding into the fuel feed stream [7,17–22], the use of more CO-tolerant electrocatalysts [8,24,25], alternating cell operating conditions [26–28], the use of a bilayer anode structure [29,30] and the of a high temperature membrane [31–33]. Among all treatments of CO poisoning, air bleeding is a simple, effective, and inexpensive approach. The effects of CO poisoning can be dramatically reduced by injected trace amount of oxygen or air (<5% air) into the anode hydrogen stream [18,23]. Many theoretical studies and models were found in the literature about CO poisoning [34–38]. These studies are summarised in Table 1. It appeared that few studies considered CO poisoning with regard to cell performance at different CO concentrations and at different amounts of air bleeding. In addition, the experimental conditions were quite varied, and no data were found in the literature on the effectiveness of air bleeding at high CO concentration (for instance, 200 ppm). Although comprehensive CO poisoning models were found in the literature, there were insufficient data for verification.

Although cell performance can be recovered by air bleeding, the effectiveness of this approach at high CO concentrations (>200 ppm) and the stability of PEMFCs subject to this treatment are not clear because of the limited available test data. The objective of this study was to provide more in-depth data on the high concentration CO poisoning issue. Experiments at high CO concentrations (up to 200 ppm) were conducted. The degradation of a PEMFC's performance due to poisoning by high CO concentrations and the recovery of its performance by air bleeding was then evaluated. A simplified mathematical model was also derived in this study. This simple model can be used to estimate the current drop and power loss due to CO poisoning under different cell temperature, cell voltage, CO concentration, and amount of air bleeding conditions. These results are important to the design and operation of reformers for residential CHP applications.

2. Experimental setup

A single PEMFC (25 cm^2) was used for all experiments. A membrane electrode assembly (MEA) consisted of two electrodes with Pt and Pt–Ru catalyst (purchased from GORE). The gas diffusion layer (GDL) used SGL 10BC carbon paper. The graphite plate was made from POCO graphite. Serpentine flow channels were fabricated on the graphite plate. Detailed specifications of the test cell and components are listed in Table 2.

A fuel cell testing station (HEPHAS, HTS-125) was used. The flow rates of the reacting gases (H_2, H_2/CO, air) were controlled using mass flow controllers (Brooks, 5850e). The reacting gas was passed through a gas bubble humidifier prior to entering the cell. The relative humidity (%RH) was determined by controlling the reacting

Table 1
Summary of experimental conditions of previous studies on CO poisoning in PEMFCs.

Year	Articles	Cell temp.	Potentiostatic mode	CO conc.	Air bleeding	CO durability test	CO poisoning model	Anode catalyst
1988	[7]	80 °C	–	5, 10, 20, 50, 100 ppm	4.5% O_2	–	–	Pt
1998	[20]	30–100 °C	–	100, 250 ppm	1–5% H_2O_2	–	–	Pt, Pt–Ru
1999	[8]	40–115 °C	–	5, 20, 50, 100 ppm	–	–	–	Pt, Pt–Ru, Pt–Sn
2001	[14]	70 °C	–	100, 1000, 10,000 ppm	–	–	–	Pt–Ru
2001	[36]	80 °C	–	25, 50, 100, 250 ppm	–	–	×	Pt
2002	[26]	80 °C	–	108 ppm	–	–	×	Pt
2002	[29]	80 °C	–	50 ppm	–	–	–	Pt, Pt–Ru
2003	[22]	70, 90 °C	–	300, 3000, 10,000 ppm	5, 10, 15% air	–	–	Pt–Ru
2003	[25]	80 °C	–	100 ppm	–	–	–	Pt, Pt–Ru
2003	[34]	–	–	–	–	–	×	Pt
2004	[28]	80–120 °C	–	10.4, 52.4, 104, 485 ppm	–	–	–	Pt–Ru
2004	[37]	80 °C	–	10, 100 ppm	–	–	×	Pt
2005	[15]	Room temp.	–	10,000 ppm	–	10.8 h	–	Pt, Pt–Ru
2006	[38]	–	–	–	–	–	×	Pt
2007	[16]	20 °C	–	1000 ppm	–	–	×	Pt–Ru
2007	[23]	60 °C	–	100 ppm	2% air	–	–	Pt
2007	[30]	65 °C	–	50 ppm	2% O_2	–	–	Ru, Pt–Ru
2007	[33]	120–180 °C	–	1%, 3%	–	–	×	Pt
2008	[19]	60 °C	0.68 V	10, 80 ppm	–	–	–	Pt–Ru
2008	[21]	70 °C	–	10 ppm	5% air	4600 h	–	Pt
2008	[35]	–	–	–	–	–	×	Pt
2009	[17]	70 °C	–	50 ppm	internal air bleed	–	×	Pt–Ru
2009	[31]	140–180 °C	–	2%, 5%	–	–	–	Pt
2010	[18]	65 °C	–	53 ppm	2–20% air	3000 h	×	Pt–Ru
2011	[24]	Room temp.	–	0, 10, 50, 100, 300, 500 ppm	–	–	–	Pt–Ru
2011	[27]	70–120 °C	–	0–200 ppm	–	–	×	Pt
2012	[32]	130–190 °C	–	2%	–	–	–	Pt
2013	[9]	60, 80 °C	–	1, 2, 10 ppm	–	200 h	–	Pt
This study		**45–85 °C**	**0.5–0.8 V**	**25, 50, 100, 200 ppm**	**1–12% air**	**300 h**	×	**Pt–Ru**

–: No.
×: Yes.

Table 2
Components and specifications of test cell.

Component items	Specifications
MEA (CCM)	GORE PRIMEA® 5621
PEM membrane	GORE SELECT®, 35 μm (thickness)
Active area	25 cm^2 (5 cm × 5 cm)
Catalyst metals	0.45 mg cm^{-2} Pt–Ru (anode) 0.6 mg cm^{-2} Pt (cathode)
GDL (carbon paper)	SGL 10BC, 410 μm (thickness)
Flow field plate (graphite)	POCO
Configuration of flow channels	Serpentine, 65 cm (length)
No. of flow channels	Two
Flow channel width/depth/interval	1 mm/1 mm/1 mm

gas dew point (VIASENSOR, HS-1000), and water produced at the cathode was separated using a gas/liquid separator. During the air bleeding experiments, the oxygen concentration was set by a computer. The injected air was automatically adjusted along with the output current of the cell. Heating pads attached to both sides of the cell were used to control the cell's temperature. Both anode and cathode current collectors were connected to electric loads (Scribner, 890e). The electrochemical impedance spectra of the cell were measured using a Scribner model 880.

A series of activation steps were applied after the cell was assembled to enable it to quickly reach a steady state. During cell activation, various cell voltages ranging from 0.9 to 0.4 V were applied for 10–20 h. Once the cell reached a steady state, experiments were started under the testing conditions summarised in Table 3. The flow rates of reacting gas were controlled at a constant stoichiometric ratio for all experiments. Under this condition, the flow rates of inlet reacting gas were automatically adjusted according to output current density. The cell temperature and cell voltage were kept at 65 °C and 0.6 V for all experiments, except during the study of CO poisoning at different cell temperatures and voltages. The anode reacting gas was a mixture of CO and H_2. The CO concentration was pre-mixed in gas cylinder; therefore constant concentration of CO could be maintained during the course of experiments. Gas cylinders with different gas compositions were ordered from a commercial gas supplier.

3. Results and discussion

The effects of CO poisoning on cell performance can be treated as a competition between the absorption reaction of hydrogen (Eq. (1)) and the absorption reaction of carbon monoxide (Eq. (2)). The catalyst surface available for hydrogen oxidation is significantly reduced by CO molecule occupation when CO is present in the hydrogen gas. Bleeding small amounts of oxygen or air into the hydrogen stream can relieve the CO poisoning effect. Oxygen absorbs on the catalyst surface where it oxidises the CO to CO_2, as observed in Eqs. (3) and (4). Here, M represents free catalyst sites and $K_{i,f}$ and $K_{i,b}$ are the rate constants of the absorption reaction and the desorption reaction of species "i". These reactions depend on many operating parameters, including cell temperature, cell voltage, and species concentration. By measuring the cell output current at various cell operating temperatures, cell voltages, CO concentrations, and amounts of air bleeding, we can establish a semi-empirical equation to describe the effects of CO poisoning at various operating conditions.

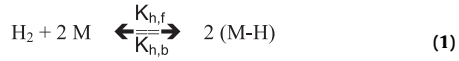

(1)

(2)

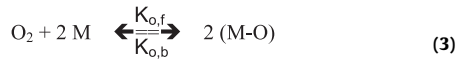

(3)

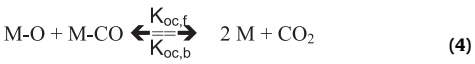

(4)

3.1. Effects of operating parameters on cell performance with CO poisoning

3.1.1. Effects of cell temperature on CO poisoning

The cell temperature is an important operating parameter with regard to fuel cell performance, and it affects the CO level that can be tolerated by the cell. Fig. 1 shows the cell current density vs. time at 0.6 V with CO poisoning subject to different operating temperatures (45, 55, 65, 75, and 85 °C). Ten minutes before the test (t = 0–10 min), the anode was fed with pure hydrogen, the current density output was very stable, and the highest current density was obtained at a cell temperature of 65–75 °C. At t = 10 min, the anode feed stream was switched from pure hydrogen to H_2 + 200 ppm CO. As shown in Fig. 1, three distinct regions were observed:

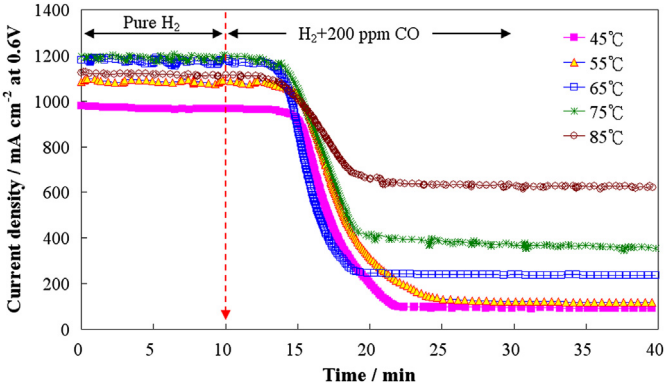

Fig. 1. Plot of cell current density responses under CO poisoning at different cell temperatures (45, 55, 65, 75, and 85 °C). The cell voltage was kept at 0.6 V and the anode feed was pure hydrogen (t = 0–10 min), followed by H_2 + 200 ppm CO (t > 10 min).

Table 3
Test conditions of PEM fuel cell.

Items	Test conditions
CO conc. in H_2 feed (anode)	25, 50, 100, 200 ppm
Cathode feed	Air
Concentration of air bleeding	1, 2, 3, 5, 7, 10, 12% air
Cell operating temperature	(1) 65 °C (2) 45, 55, 65, 75, 85 °C
Cell operating voltage	(1) 0.6 V (2) 0.8, 0.7, 0.6, 0.5 V
Stoich. ratio of H_2, air	1.5×, 3.0×
Humidity of H_2, air	100 %RH
Pressure of H_2, air	Ambient pressure
EIS test	Frequency range (10 kHz–0.1 Hz), Amplitude (5 mV)

(1) During the initial stage of 200 ppm CO injection, the cell performance was not immediately affected by the introduction of CO because of the inherent time delay for diffusion of CO through the gas diffusion layer (GDL).
(2) A transition behaviour was observed approximately 5–20 min after CO injection when the cell output current density quickly dropped to a low level. During this period, the CO molecules had diffused to the catalyst layer and been absorbed on active sites. When the CO molecules reach the Pt catalyst layer, CO is adsorbed and occupies the Pt catalyst sites. The binding strength of CO on Pt is stronger than that for H_2 on Pt, resulting in the catalyst surface quickly becoming covered by CO, the catalyst losing its activity and the cell performance being degraded accordingly.
(3) A stable low current density was obtained approximately 20 min later ($t = 30$ min), when the cell output current density reached another stable value. The new stable value of current density (i_{ss}) increased with the cell temperature. For instance, the values of i_{ss} at cell temperatures of 45, 55 and 85 °C were 94, 122, and 630 mA cm^{-2}, respectively.

Therefore, the CO tolerance level was shown to increase with the cell's operating temperature. However, the proton-exchange membrane (PEM) may dry out and lose its proton conductivity if the cell temperature is too high (>80 °C). From these results, we can conclude that operating a cell at a temperature 5–10 °C higher than the pure hydrogen feed not only improves cell performance but also reduces the CO poisoning effect. Similar CO poisoning behaviour was also observed in the literature [8,20,28]. The CO poisoning effect is reduced as the operating temperature increased. The results suggest that a high temperature leads to more CO desorption rather than CO adsorption. Li et al. [34,35] proposed a comprehensive model, suggesting that CO adsorption/desorption follows a Temkin model. Increasing operating pressure or temperature then mitigates CO poisoning. Lee et al. [8] compared the CO poisoning effects among Pt/C, Pt–Ru/C, and Pt–Sn/C catalysts at cell temperatures of 40, 55, 70, 85, 100, and 115 °C. The electrode potential shift in the polarisation curve for hydrogen oxidation was in the order of Pt–Sn/C < Pt–Ru/C < Pt/C. A binary catalyst had a better CO tolerance than a Pt catalyst alone.

3.1.2. Effects of cell voltage on CO poisoning

The open circuit voltage (OCV) of the PEMFC was approximately 0.9–1.0 V. To obtain a high power density, the actual operating cell voltage was approximately 0.6–0.7 V. Fig. 2 shows the change in current density with time at the constant potential and 65 °C, subjected to various cell voltages (0.5–0.8 V). Before the CO poisoning test, the anode fuel was pure hydrogen ($t = 0$–10 min), and the output current densities at cell voltages of 0.8, 0.7, 0.6, and 0.5 V were very stable at 130, 600, 1095, and 1560 mA cm^{-2}, respectively. When 200 ppm CO was introduced into the hydrogen fuel stream ($t > 10$ min), the output current density rapidly decreased in a few minutes. The degradation rate of current density increased as the cell operating voltage decreased because the cell was operating at a constant stoichiometric ratio. The flow rate of anode fuel was adjusted according to the output current. At a high cell voltage, the current density was low, and the CO-containing fuel was accordingly maintained at a low flow rate. Conversely, the current density was high at a low cell voltage, and the CO-containing fuel was maintained at a high flow rate. Approximately 20 min later ($t = 30$ min), the current density reached new steady state values (i_{ss}) of 74, 216, and 353 mA cm^{-2} for cell voltages of 0.8, 0.6, and 0.5 V, respectively. Therefore, the cell voltage, current density and stoichiometric ratio of fuel are important factors when considering how to improve the CO tolerance level of a fuel cell.

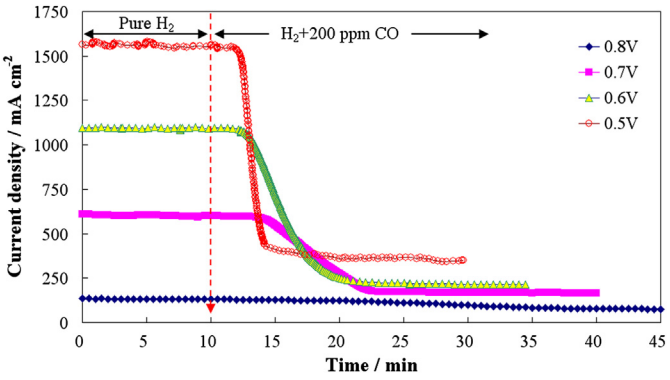

Fig. 2. Current density response during potentiostatic operation at 65 °C and different cell voltages (0.8, 0.7, 0.6, and 0.5 V). The anode feed was pure hydrogen ($t = 0$–10 min), followed by H_2 + 200 ppm CO ($t > 10$ min).

3.1.3. Effects of CO concentration on cell performance

Fig. 3 shows the cell current density responses in time to CO poisoning at 0.6 V/65 °C and hydrogen feed stream containing different CO concentrations (25–200 ppm). The experimental sequence for the anode feed stream was pure hydrogen first, followed by feeding the fuel gas in which different concentration of CO was mixed with H_2 in advance. Using the pure hydrogen feed ($t = 0$–10 min), the average cell current density was approximately 1265 mA cm^{-2}. The cell current density quickly dropped to a new steady state value (i_{ss}) after the fuel containing CO was introduced. This suggested that the absorption/desorption of CO on Pt active sites were at their equilibrium state. The time (t_{ss}) for the cell to reach the new steady state current density (i_{ss}) was short for hydrogen with a high CO concentration. The required time to reach the steady state, t_{ss}, were 40 and 15 min for CO concentrations of 25 and 200 ppm, respectively. This result is similar to data obtained by Bhatia and Wang [37] and Sung et al. [18]. Bhatia and Wang [37] proposed a lumped model of hydrogen and CO adsorption, desorption, and electro-oxidation coupled with a current–voltage relationship for fuel cell performance. Their model reasonably agreed with measured data. Sung et al. [18] modified Zamel and Li's model [35] to include the recovery of cell performance because of air bleeding. This model fitted the measured data very well.

Table 4 lists the steady state current density and CO sensitivity for different CO concentrations. The CO sensitivity (S_{CO}) was calculated using Eq. (5) and is the ratio of the change of steady state current density to the CO concentration (C_{CO}, in ppm).

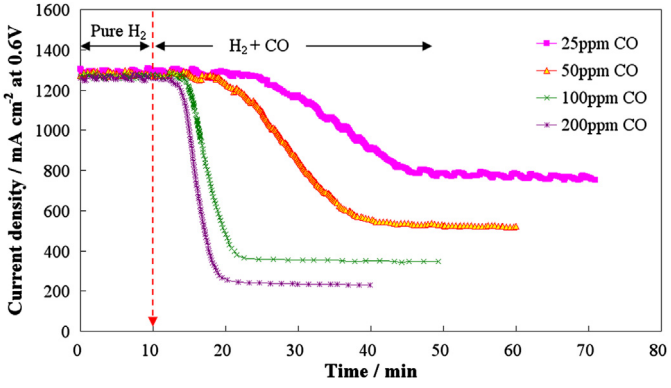

Fig. 3. Plot of cell current density responses under CO poisoning at 0.6 V and 65 °C. The anode feed was pure hydrogen ($t = 0$–10 min), followed by different CO concentrations (25, 50, 100, 200 ppm) into the anode fuel stream ($t > 10$ min).

Table 4
Sensitivity of the cell current density to CO concentration.

CO concentration (ppm)	Steady state current density (mA cm^{-2})	Sensitivity (S_{CO})
0	1265	
25	770	19.8
50	530	14.7
100	355	9.1
200	240	5.1

$$S_{CO} = \frac{i_{ss}^{0} - i_{ss}^{co}}{C_{CO}} \quad (5)$$

In the equation above, i_{ss}^{0} is the steady state current density with pure hydrogen feed, and i_{ss}^{co} is the current density of CO-containing hydrogen. Table 4 shows the cell current density was more sensitive at low CO concentrations than at high CO concentrations. Although the anode of this cell used a CO-tolerant catalyst (Pt–Ru), the cell performance was sensitive to CO poisoning after a short time, even at a low CO level (25 ppm).

3.1.4. Effects of air bleeding on CO poisoning

Fig. 4 shows the cell current density at 0.6 V and various levels of air bleeding (1–12%) when the anode fuel contained 200 ppm CO. When the anode was fed with H_2/CO, the cell current density decreased from 1290 mA cm^{-2} to 245 mA cm^{-2} within 25 min. However, the CO poisoning effect could be reversed by injecting a small amount of air into the anode fuel stream. The cell current density then quickly increased because the oxygen in the air quickly oxidised the CO absorbed on the Pt catalyst surface to CO_2 ($CO + 1/2O_2 \rightarrow CO_2$). With the adsorbed CO removed, the active sites on Pt catalyst were free to adsorb hydrogen that in turn could be oxidised ($H_2 \rightarrow 2H^+ + 2e^-$). This approach is known as anode air bleeding.

As observed in Fig. 4, when the anode feed was injected with 1% air, the current density quickly increased from 245 to 500 mA cm^{-2}.

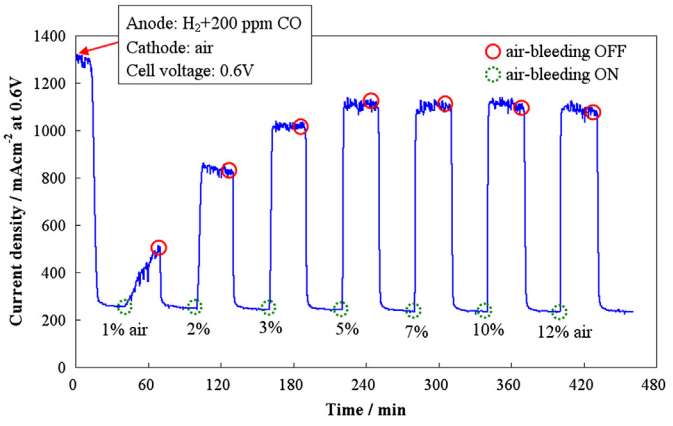

Fig. 4. Effects of air bleeding on the cell current density in a CO-poisoned fuel cell. The cell was operated at 0.6 V/65 °C and various levels of air bleeding (1–12%). The hydrogen containing 200 ppm CO was introduced at $t = 0$ min.

The current density increased to 1020 mA cm^{-2} when 3% air was injected into the anode stream and reached 1105 mA cm^{-2} when 5% air was injected. The improvement of current density gradually diminished when the amount of injected air was increased from 5% to 10%, and the current density was observed to decrease when the amount of injected air exceeded 10%. This may have occurred because injecting a large amount of air into the anode fuel stream dilutes the hydrogen and because some of the hydrogen may be oxidised by the oxygen in the air and thus not contribute to power generation.

In summary, the cell output current density or power density is heavily dependent on several operating parameters, including cell temperature (T), cell voltage (E), CO concentration (C_{CO}), and bleeding air concentration (C_{air}). A semi-empirical equation is proposed to model the effects of operating parameters on the cell output current density. As given by Eq. (6), the modelled net current density (i_{net}) output from the cell contains three parts:

a. the current density due to the hydrogen oxidation reaction (i_{H_2}),
b. the current density reduction due to CO poisoning (i_{CO}), and
c. the current density recovery due to air bleeding (i_{air}).

Both i_{H_2} and i_{CO} are expressed as functions of T, E, C_{CO}, and C_{air}. The Arrhenius equation is used to account for the temperature effects on both reactions, and the Tafel equation is used to account for the voltage effects on both reactions. The model assumes that the CO adsorption reaction is proportional to CO concentration (C_{CO}) with reaction order (n_{CO}) and that the current density recovery due to air bleeding (i_{air}) is the interaction between CO and O_2 molecules. Therefore, the recovered current density is proportional to C_{CO} with respect to the CO reaction order n_{CO} and to C_{air} with respect to the O_2 reaction order n_{air}.

$$\begin{aligned} i_{net} &= i_{H_2} - i_{CO} + i_{air} \\ &= i_{H_2}^{o} \cdot \exp\left[-\Delta G_{H_2}/RT\right] \cdot \exp\left[-\alpha_{H_2} F\left(E - E_{H_2}^{o}\right)/RT\right] - i_{CO}^{o} \cdot C_{CO}^{n_{CO}} \cdot \exp\left[-\Delta G_{CO}/RT\right] \cdot \exp\left[-\alpha_{CO} F\left(E - E_{CO}^{o}\right)/RT\right] + i_{air}^{o} C_{CO}^{n_{CO}} C_{air}^{n_{air}} \end{aligned} \quad (6)$$

Here ΔG_{H_2} and ΔG_{CO} are the activation energies of the hydrogen oxidation and CO adsorption reactions, respectively. $i_{H_2}^{o}$, i_{CO}^{o}, i_{air}^{o} are the exchanging current densities of the hydrogen oxidation, the CO adsorption, and the oxygen and CO recovery reactions, respectively. $E_{H_2}^{o}$ and E_{CO}^{o} are the equilibrium potentials of the hydrogen oxidation and CO adsorption reactions, respectively. α_{H_2} and α_{CO} are the charge transfer coefficients for the hydrogen oxidation and CO adsorption reactions, respectively. The parameters in Eq. (6) are calculated based on the data measured in this work and are listed Table 5. The calculated results of the proposed model are compared with experimental data in Fig. 5(a) as a function of the cell temperature, in Fig. 5(b) as a function of the cell voltage, in Fig. 5(c) as a function of the CO concentration, and in Fig. 5(d) as a function of

Table 5
Parameter values used in the modelling.

Hydrogen (H_2)	Carbon monoxide (CO)	Air bleeding (O_2)
	$n_{CO} = 0.36$	$n_{air} = 0.27$
$\alpha_{H_2} = 0.13$	$\alpha_{CO} = 0.13$	
$i_{H_2}^{o} = 6.0 \times 10^{5}$	$i_{CO}^{o} = 4.8 \times 10^{3}$	$i_{air}^{o} = 75$
$\Delta G_{H_2}^{o} = 2.6 \times 10^{4}$	$\Delta G_{CO}^{o} = 4.3 \times 10^{4}$	
$E_{H_2}^{o} = 1.23$	$E_{CO}^{o} = 3.2$	

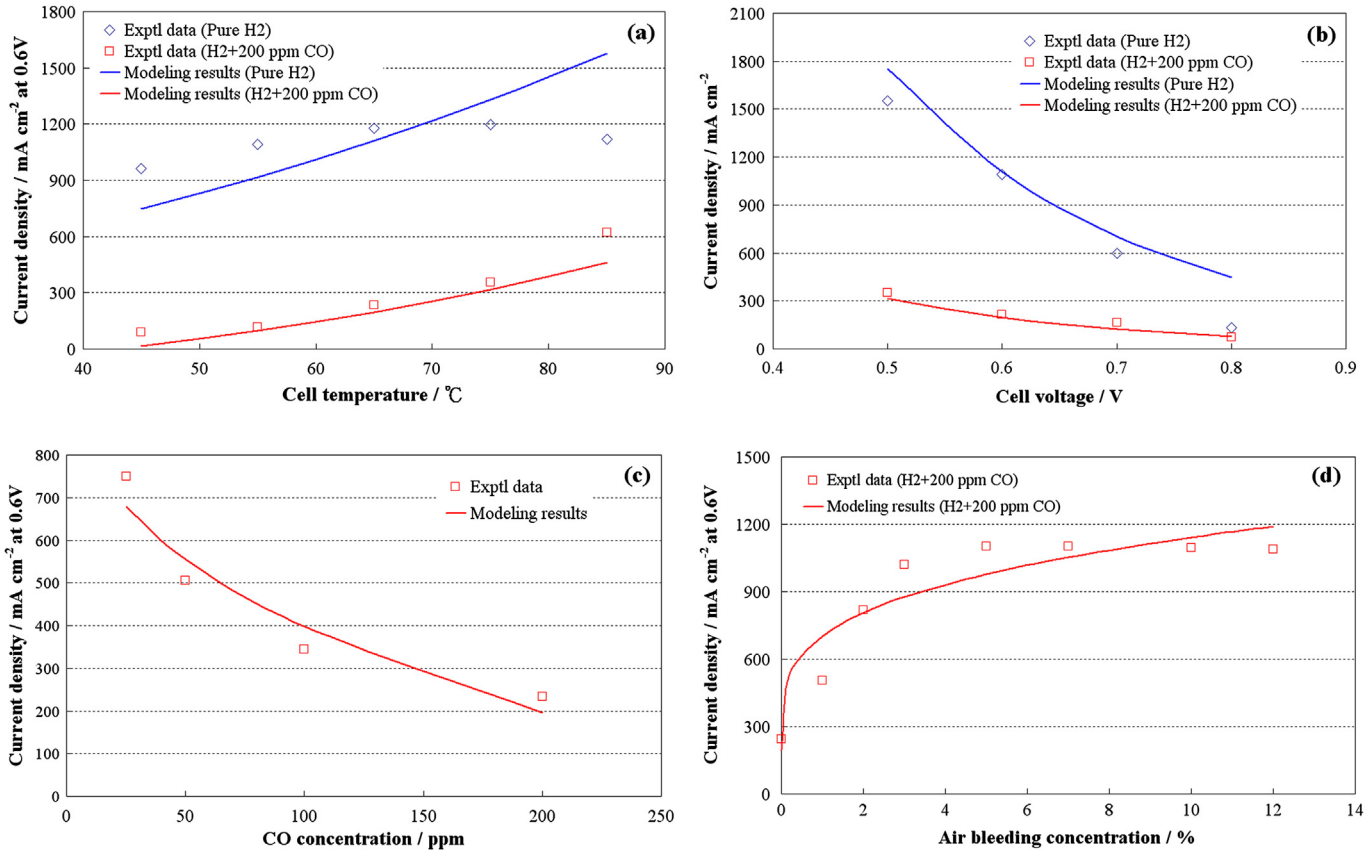

Fig. 5. Comparison among experimental data from Figs. 1–4 and modelling results from Eq. (6). (a) As a function of cell temperature, (b) as a function of cell voltage, (c) as a function of CO concentration, (d) as a function of air bleeding concentration.

the air bleeding concentration. The calculated results are in reasonable agreement with experimental data, except the cell temperature dependence (Fig. 5(a)) where the modelling results differed from the experimental data. This deviation may be due to the PEM membrane dehydration at the high cell temperature (>80 °C). Cells with dehydrated membranes have reduced performances [39].

3.2. Cell performance effects of CO in the hydrogen stream

3.2.1. I–V polarisation measurement

The *I–V* polarisation curve was obtained using the voltage controlling mode. The cell voltage was step-changed from the open circuit voltage (OCV) down to 0.5 V. The inlet gas flow rates were controlled at a constant stoichiometric ratio and were changed based on the cell current density. The steady state currents were recorded and are shown in Fig. 6. In the PEMFC, the rate of the anode hydrogen oxidation is much faster than the rate of O_2 reduction on the cathode. Therefore, the major portion of the cell voltage loss is due to the cathode overpotential, while the anode overpotential can be ignored. When CO (at the ppm level) is introduced into the anode fuel stream, severe CO poisoning occurs on the anode. The anode overpotential may be greater than the cathode overpotential, depending on the CO concentration. In this CO poisoning situation, the cell voltage loss is attributed to both anode and cathode overpotential. With a constant cathode operating condition, the variation of cell voltage observed here was due to the introduction of CO in the anode fuel.

Fig. 6 shows the steady state *I–V* polarisation for various CO poisoning conditions (25–200 ppm), with the cell temperature at 65 °C and using air as the cathode gas. Good cell output current density was obtained using pure hydrogen. However, the cell performance decayed significantly when the hydrogen fuel contained a trace amount of CO at the ppm level. At a cell voltage of 0.5 V, the current density dropped from 1770 mA cm^{-2} to 920, 510, and 315 mA cm^{-2} when the hydrogen fuel contained 25, 100, and 200 ppm CO, respectively. These corresponded to declines of 48%, 71.2%, and 82.2%, respectively, in the original current density. In a high voltage range (>0.8 V), the addition of CO up to 200 ppm had a minor effect on current density. In a low voltage range (<0.8 V), the addition of CO caused a significant reduction in current density.

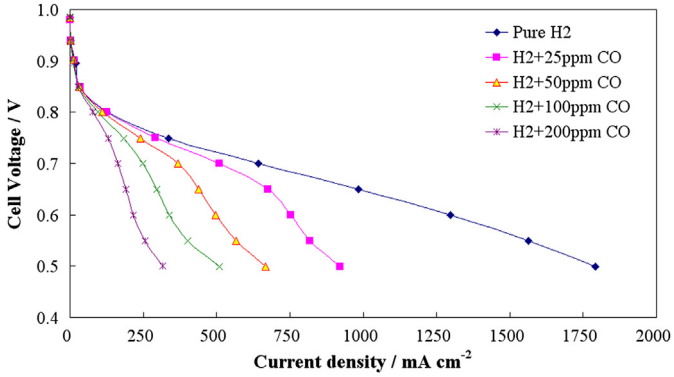

Fig. 6. Steady state *I–V* polarisation curves with hydrogen fuel containing different CO concentrations (25, 50, 100 and 200 ppm). The cell temperature was 65 °C, and air was used as the cathode gas.

In 1988, Gottesfeld and Pafford [7] were early investigators on the CO poisoning effects (5–100 ppm levels) on PEMFC. They found that the polarisation curve shows negligible effects at very low current densities, followed by a strong increase in polarisation at high current densities. Similar *I–V* polarisation curves were obtained by Springer et al. [36] with pure hydrogen, and hydrogen containing CO concentrations of 25, 50, 100, and 250 ppm at a cell temperature of 80 °C. Similar observations about polarisation curves were found among literature data [7,28,36], modelling results [34], and our data. As shown in Fig. 6, a small voltage loss in the low current density range was due to the addition of CO to hydrogen, followed by a much steeper decline in cell voltage and eventual levelling off at an almost constant, low cell voltage. The voltage loss in high cell voltage region (around 0.8–0.9 V) was independent of CO concentration. It might be due to low CO adsorption in this region. Effect of CO adsorption on activation overpotential is minor. However, in low cell voltage region (<0.8 V), CO adsorption becomes significant and the influence of CO on activation overpotential is important.

3.2.2. *In situ EIS measurement*

The electrochemical impedance spectroscopy (EIS) of the cell was measured to elucidate the CO poisoning at the anode. The measurements were conducted on a single cell, whose anode fuel contained different CO concentrations, after the cell had reached a steady state condition. As shown in Fig. 7, a simplified equivalent circuit model, $R_1(R_2C_2)$ was used to represent the behaviour of the EIS data. The internal resistance of the cell (R_1) was connected in series with a parallel R_2C_2 circuit. This R_2C_2 circuit accounted for the impedance due to oxygen reduction on the cathode and hydrogen oxidation on the anode. The cell impedance could be ignored when the anode fuel was pure hydrogen. However, it became the major portion of the cell impedance when the anode was poisoned by CO.

The Nyquist plots of the cell at different levels of CO poisoning concentrations (i.e., 25, 50, 100, and 200 ppm), under steady state conditions of 65 °C and a cell voltage 0.6 V, are shown in Fig. 7. During the impedance measurement, the frequency was scanned from 10 kHz to 0.1 Hz. The EIS curve appeared as a semi-circle with two intercepts on the *X* axis. The EIS curve intersected the *X* axis at R_1 in the high frequency region and at $R_1 + R_2$ in the low frequency region. The R_1 is the cell's internal resistance, which is approximately 2.62 mΩ for all CO concentrations (25–200 ppm). As expected, the cell's internal resistance is not affected by the amount of CO in the anode hydrogen fuel. The value of R_2 is the charge transfer resistance due to the oxygen reduction reaction (ORR) and the hydrogen oxidation reaction (HOR). The R_2 at the zero CO concentration, R_2o, represents the cell impedance caused by the ORR/HOR and has a value of 11.4 mΩ. The difference between R_2 and R_2o, ΔR_2 is the increment of R_2 due to CO poisoning. Values of ΔR_2 are 6.4, 33, and 72 mΩ for CO concentrations of 25, 100, and 200 ppm, respectively. Therefore, the implicit dynamic response of the cell impedances shows that the degradation of fuel cell performance during poisoning with CO is dominated by an increase in charge transfer resistance. An induction behaviour in the EIS low frequency region was observed by Wagner and Schulze [25]. They suggested that the increasing pseudo-inductive behaviour was due to a surface relaxation process caused by CO at the anode. This induction behaviour was also observed in a methanol oxidation

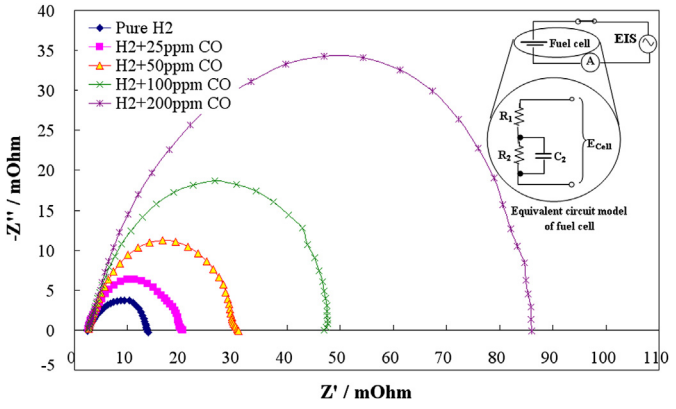

Fig. 7. Nyquist plots of EIS measured at steady state, operating at 65 °C/0.6 V during CO poisoning with anode fuel containing different CO concentrations (25, 50, 100, 200 ppm).

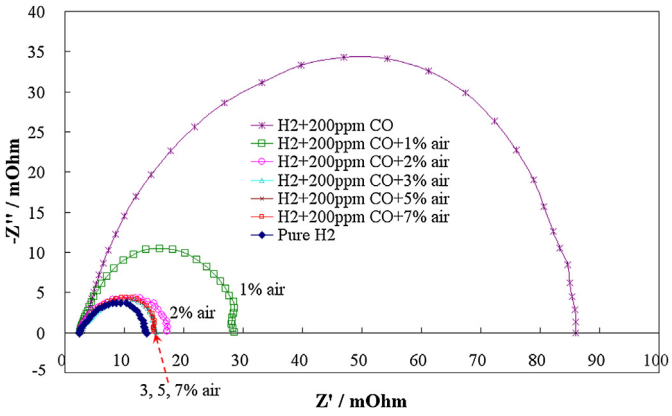

Fig. 8. Nyquist plots of EIS measured at steady state, operating at 65 °C/0.6 V and anode fuel containing 200 ppm CO with different levels air bleeding (1, 2, 3, 5 and 7% air).

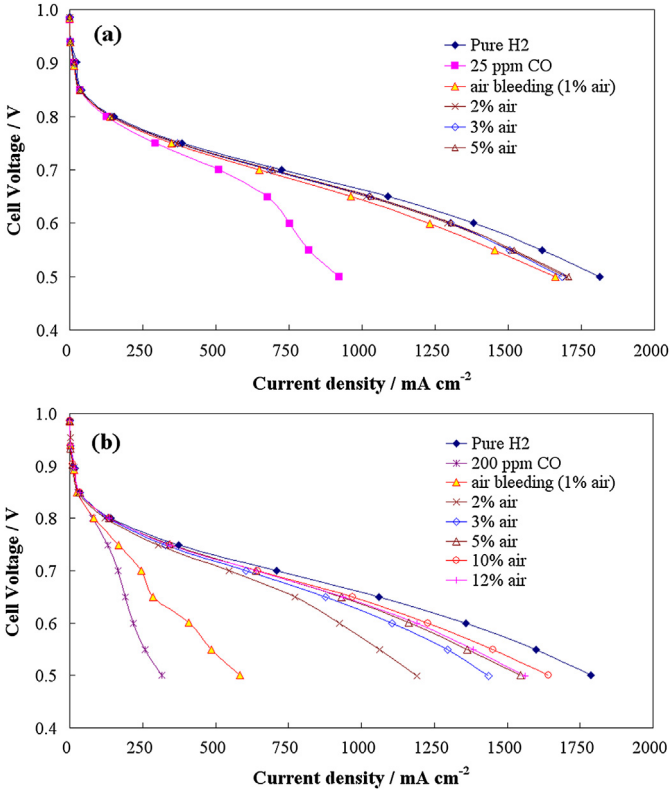

Fig. 9. *I–V* polarisation curves under various air bleeding conditions. The anode fuel stream consisted of H_2/CO and different concentrations of air. (a) Air bleeding with hydrogen fuel containing 25 ppm CO, (b) air bleeding with hydrogen fuel containing 200 ppm CO.

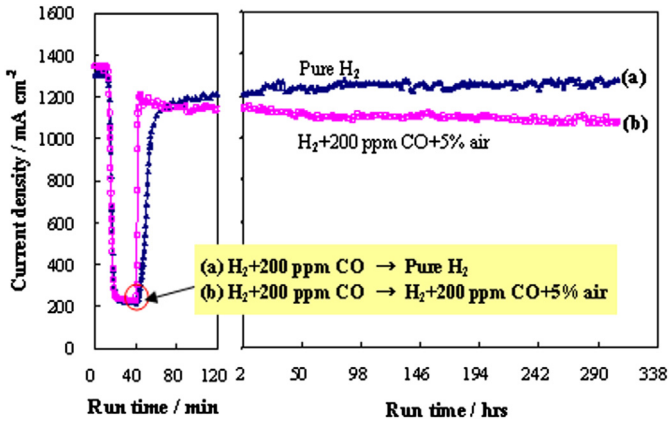

Fig. 10. A 300-h stability test of the PEMFC at 65 °C/0.6 V. The anode was fed with (a) H_2 + 200 ppm CO → Pure H_2, (b) H_2 + 200 ppm CO → H_2 + 200 ppm CO + 5% air.

reaction where CO adsorption was an intermediate step [40]. With a small amount of air injection into the anode fuel stream, the charge transfer resistance was significantly reduced as shown in Fig. 8. The CO poisoning level in fuel cells can be revealed from the changes in the charge transfer resistance. For CO-containing anode fuel (H_2 + 200 ppm CO), with 1% air bleeding, the cell charge transfer resistance (R_2) was reduced from 83.3 mΩ to 26 mΩ. The value of R_2 was further reduced to 13.5 mΩ when the anode was injected with 2% air. The effects of air bleeding on cell performance recovery became less significant at higher percentage air bleeding (>2% air). This suggested that most of the CO on the catalyst was removed by 2% air bleeding.

3.3. Effects of anode air bleeding on cell performance

Fig. 9(a) and (b) shows the *I*–*V* polarisation curves under various levels of air bleeding (1–12%) into anode fuel containing 25 and 200 ppm CO, respectively. Data were collected after the cell had reached a steady state. It was shown that even a trace amount of CO can cause severe decay in the cell performance, as shown in Fig. 6. However, the cell performance could be recovered with a small amount of air into the anode fuel stream. For instance, at a cell voltage of 0.5 V with fuel that contained 25 ppm CO, the output current density was 920 mA cm^{-2}, but it could be significantly recovered to 1670 mA cm^{-2} by addition of only 1% air into the anode fuel. For fuel containing 200 ppm CO, the current density increased from 315 to 1600 mA cm^{-2} by adding 5% air into the anode fuel. These results showed that the power density of the cell could be improved by more than 88%. However, when the amount of air introduced into the anode fuel was more than 10%, the cell's current density was observed to decrease. This phenomenon was consisted with our previous experimental results as shown in Fig. 4. Inaba et al. [21] found that the oxygen on the anode side not only reacted with CO, but it also generated hydrogen peroxide (H_2O_2) during air bleeding. H_2O_2 attacks electrodes and PEM membranes. The presence of H_2O_2 thus accelerates the degradation of a proton-exchange membrane and cell performance. The amount of air used in air bleeding should be adjusted based on the CO concentration because excessive air bleeding will not only dilute the hydrogen concentration in the fuel stream but will also reduce PEMFC operating life.

3.4. Effects of anode air bleeding on long-term stability

From the results and analyses discussed above, it is clear that air bleeding into the hydrogen fuel stream is an effective approach to relieving CO poisoning for PEMFCs. Even at a high CO concentration (200 ppm), 5% air bleeding can recover the cell performance to 90% of its original value within 10 min. However, all the tests were conducted over a period of several hours. The effects of air bleeding on durability and stability are still unclear, and there is little detailed discussion of this issue in the literature. Therefore, the present study also conducted a 300-h stability study of air bleeding in a CO-poisoned cell (200 ppm CO). Experimental results are shown in Fig. 10.

From Fig. 10, the cell's current density is shown to decay by 82% (from 1320 to 240 mA cm^{-2}) within 30 min when the 200 ppm CO was introduced into the anode fuel. After CO poisoning for 30 min (t = 40 min), one cell had 5% air injected into the anode fuel while anode stream in the other cell was switched to pure hydrogen. The current density for the cell with the air bleeding treatment recovered much faster than the cell with the pure hydrogen treatment. Within 4 min, the current density increased to 1200 mA cm^{-2} with a 5% air bleeding while the cell with pure hydrogen treatment required 60 min. By switching CO/H_2 to pure hydrogen, the adsorbed CO is desorbed slowly and the recovery of cell performance was slow. In air bleeding, the oxygen is reacted with adsorbed CO on the catalyst. The adsorbed CO is removed quickly.

At the end of the 300-h test, the cell subjected to air bleeding had recovered up to 80% of its original current density. During the testing period, the cell current density was maintained in a fairly stable range (1105–1140 mA cm^{-2}). The degradation in the average current density during the test was very small (<2%). At a high CO concentration (200 ppm), 5% air bleeding was sufficient to minimise the effects of CO poisoning on cell performance. We also found that the cell subjected to pure hydrogen treatment did not recover its original current density. This finding may be due to incomplete removal of CO that was adsorbed on the Pt catalyst or aggregation

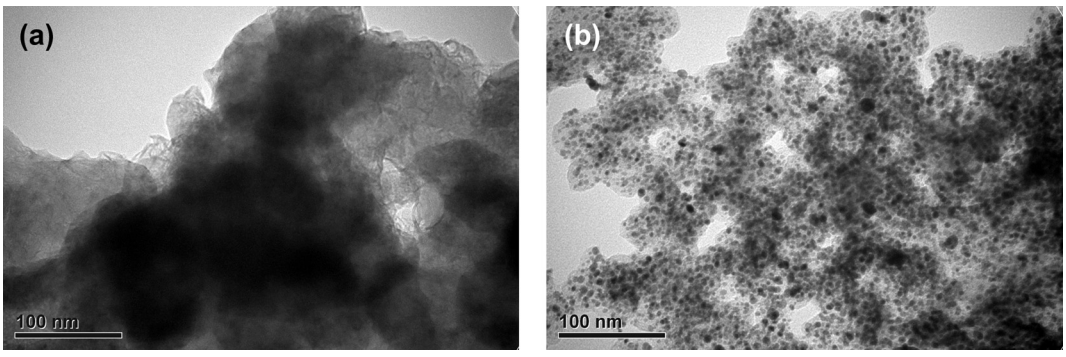

Fig. 11. TEM images of anode catalyst. (a) Catalyst before test, (b) catalyst after 300 h long-term duration test.

of the Pt–Ru catalyst. Fig. 11 shows TEM images of the anode catalyst (Pt–Ru), where the particle size of the catalyst was significantly enlarged or aggregated after long-term duration test. This may explain why the cell performance was not recovered to its original performance at the end of the duration test.

4. Conclusions

This study used a single PEMFC to investigate CO poisoning phenomena under various operating conditions (i.e., cell temperature, CO concentration, cell voltage, and air bleeding) and the effectiveness of anode air bleeding to mitigate CO poisoning. A simplified mathematical model was proposed to account for CO poisoning behaviour at all tested operating conditions and for recovery by air bleeding. The predictive results from the simplified model are in reasonable agreement with the experimental data. This fuel cell performance model can be further expanded for simulation and optimisation of CHP systems in the future. Under CO poisoning conditions, severe current density decay occurred, even when the anode fuel contained CO as low as 25 ppm and a CO-tolerant catalyst (Pt–Ru) was used. The test results show that a small variation of CO concentration (0–200 ppm) in hydrogen fuel stream will cause a huge reduction of power output from a PEMFC (0.65–0.13 W cm^{-2} at 0.65 V). Cells operated at high temperatures (>60 °C) had better CO tolerance than cells operated at lower temperatures. A significant current reduction due to CO poisoning was observed in the lower voltage range (<0.8 V). From the EIS results, it was determined that the presence of CO mainly increased the impedance of charge transfer and affected less on the cell's internal resistance. A small amount of air bleeding effectively recovered the cell's original performance, even for fuel containing a high concentration of CO (200 ppm). With 5–7% air bleeding, the cell performance recovered up to 90% of its original value within 10 min. A 300-h stability test indicated that 5% air bleeding could recover most of the cell performance (from 240 to 1100 mA cm^{-2}). The cell generated a relatively stable output throughout the stability test and it showed a minor degradation (<2%) after 300 h. The power output of a PEMFC system with air bleeding is more tolerant to changes in the CO concentration than a system without it. However, excessive air bleeding (>10% air) may adversely affect the performance. Air bleeding induces the combustion reaction of adsorbed CO and oxygen. This combustion reaction is an exothermic chemical reaction. Additional thermal load is added onto the catalyst which could accelerate the aggregation of catalyst. Air bleeding should be performed with caution. For a PEMFC power system with hydrogen-rich reformate gas generated from a reformer, air bleeding offers two unique advantages in practice. First, a power system with air bleeding is able to deliver a more stable power output. Secondly, a power system with an air bleeding design can adopt a simpler, smaller, and cheaper reformer.

Acknowledgements

The authors wish to express their appreciation for financial support from the Bureau of Energy of the Ministry of Economical Affairs (MOEA), the National Science Council (NSC), and the National Taiwan University of Science and Technology, Taiwan. Experimental work was performed at the Fuel Cell Laboratory of GEL/ITRI (Green Energy and Environmental Research Laboratories/Industrial Technology Research Institute).

References

[1] E.M. Assaf, J.M. Assaf, J. Power Sources 196 (2011) 747–753.
[2] H.S. Chu, F. Tsau, Y.Y. Yan, K.L. Hsueh, F.L. Chen, J. Power Sources 176 (2008) 499–514.
[3] N. Briguglio, M. Ferraro, G. Brunaccini, V. Antonucci, Int. J. Hydrogen Energy 36 (2011) 8028–8029.
[4] M.F. Torchio, M.G. Santarelli, A. Nicali, J. Power Sources 149 (2005) 33–43.
[5] P.V. Gosavi, R.B. Biniwale, J. Power Sources 222 (2013) 1–9.
[6] D.L. Trimm, Appl. Catal. A: Gen. 296 (2005) 1–11.
[7] S. Gottesfeld, J. Pafford, J. Electrochem. Soc. 135 (1988) 2651–2652.
[8] S.J. Lee, S. Mukerjee, E.A. Ticianelli, J. McBreen, Electrochim. Acta 44 (1999) 3283–3293.
[9] G. Bender, M. Angelo, K. Bethune, R. Rocheleau, J. Power Sources 228 (2013) 159–169.
[10] H. Igarashi, H. Uchida, M. Suzuki, Y. Sasaki, M. Watanabe, Appl. Catal. A: Gen. 159 (1997) 159–166.
[11] M.J. Kahlich, H.A. Gasteiger, R.J. Behm, J. Catal. 171 (1997) 93–105.
[12] V. Galvita, K. Sundmacher, Chem. Eng. J. 134 (2007) 168–174.
[13] Z.W. Dunbar, D. Chu, J. Power Sources 217 (2012) 47–53.
[14] L.P.L. Carrette, K.A. Friedrich, M. Huber, U. Stimming, Phys. Chem. Chem. Phys. 3 (2001) 320–324.
[15] W.A. Adams, J. Blair, K.R. Bullock, C.L. Gardner, J. Power Sources 145 (2005) 55–61.
[16] C.G. Farrell, C.L. Gardner, M. Ternan, J. Power Sources 171 (2007) 282–293.
[17] W. Wang, J. Power Sources 191 (2009) 400–406.
[18] L.Y. Sung, B.J. Hwang, K.L. Hsueh, F.H. Tsau, J. Power Sources 195 (2010) 1630–1639.
[19] T. Tingelof, L. Hedstrom, N. Holmstrom, P. Alvfors, G. Lindbergh, Int. J. Hydrogen Energy 33 (2008) 2064–2072.
[20] J. Divisek, H.F. Oetjen, V. Peinecke, V.M. Schmidt, U. Stimming, Electrochim. Acta 43 (1998) 3811–3815.
[21] M. Inaba, M. Sugishita, J. Wada, K. Matsuzawa, H. Yamada, A. Tasaka, J. Power Sources 178 (2008) 699–705.
[22] M. Murthy, M. Esayian, W.K. Lee, J.W.V. Zeeb, J. Electrochem. Soc. 150 (2003) A29–A34.
[23] W. Shi, M. Hou, Z. Shao, J. Hu, Z. Hou, P. Ming, B. Yi, J. Power Sources 174 (2007) 164–169.
[24] L. Zhang, J. Kim, H.M. Chen, F. Nan, K. Dudeck, R.S. Liu, G.A. Botton, J. Zhang, J. Power Sources 196 (2011) 9117–9123.
[25] N. Wagner, M. Schulze, Electrochim. Acta 48 (2003) 3899–3907.
[26] J. Zhang, T. Thampan, R. Datta, J. Electrochem. Soc. 149 (2002) A765–A772.
[27] L. Barelli, G. Bidini, F. Gallorini, A. Ottaviano, Int. J. Hydrogen Energy 36 (2011) 10434–10442.
[28] Y. Si, R. Jiang, J.C. Lin, H.R. Kunz, J.M. Fenton, J. Electrochem. Soc. 151 (2004) A1820–A1824.
[29] H. Yu, Z. Hou, B. Yi, Z. Lin, J. Power Sources 105 (2002) 52–57.
[30] C.H. Wan, Q.H. Zhuang, Electrochim. Acta 52 (2007) 4111–4123.
[31] S.K. Das, A. Reis, K.J. Berry, J. Power Sources 193 (2009) 691–698.
[32] J.J. Linares, C. Sanches, V.A. Paganin, E.R. Gonzalez, Int. J. Hydrogen Energy 37 (2012) 7212–7220.
[33] C.P. Wang, H.S. Chu, Y.Y. Yan, K.L. Hsueh, J. Power Sources 170 (2007) 235–241.
[34] J.J. Baschuk, X. Li, Int. J. Energy Res. 27 (2003) 1095–1116.
[35] N. Zamel, X. Li, Int. J. Hydrogen Energy 33 (2008) 1335–1344.
[36] T.E. Springer, T. Rockward, T.A. Zawodzinski, S. Gottesfeld, J. Electrochem. Soc. 148 (2001) A11–A23.
[37] K.K. Bhatia, C.Y. Wang, Electrochim. Acta 49 (2004) 2333–2341.
[38] H.S. Chu, C.P. Wang, W.C. Liao, W.M. Yan, J. Power Sources 159 (2006) 1071–1077.
[39] C. Yang, S. Srinivasan, A.B. Bocarsly, S. Tulyani, J.B. Benziger, J. Membr. Sci. 237 (2004) 145–161.
[40] K.L. Hsueh, C.M. Lai, C.P. Hwang, F.C. Wu, L.D. Tsai, Y.M. Peng, J.C. Li, ECS Trans. 1 (2006) 323–330.